

The concentration-velocity dispersion relation in galaxy groups

Andreas Faltenbacher^{1,2} and William G. Mathews²

¹ *Shanghai Astronomical Observatory, 80 Nandan Road, Shanghai 200030, China*

² *UCO/Lick Observatory, University of California at Santa Cruz, 1156 High Street, Santa Cruz, CA 95064, USA*

11 June 2021

ABSTRACT

Based on results from cold dark matter N-body simulations we develop a dynamical model for the evolution of subhaloes within group sized host haloes. Only subhaloes more massive than $5 \times 10^8 M_\odot$ are considered, because they are massive enough to possibly host luminous galaxies. On their orbits within a growing host potential the subhaloes are subject to tidal stripping and dynamical friction. At the present time ($z = 0$) all model hosts have equal mass ($M_{vir} = 3.9 \times 10^{13} M_\odot$) but different concentrations associated with different formation times. We investigate the variation of subhaloe (or satellite galaxy) velocity dispersion with host concentration and/or formation time. In agreement with the Jeans equation the velocity dispersion of subhaloes increases with the host concentration. Between concentrations ~ 5 and ~ 20 the subhaloe velocity dispersions increase by factor of ~ 1.25 . By applying a simplified tidal disruption criterion, i.e. rejection of all subhaloes with a tidal truncation radius below 3 kpc at $z = 0$, the central velocity dispersion of the 'surviving' subhaloe sample increases substantially for all concentrations. The enhanced central velocity dispersions in the surviving subhaloe samples are caused by a lack slow tangential motions. Additionally, we present a fitting formula for the anisotropy parameter which does not depend on concentration if the group-centric distances are scaled by r_s , the characteristic radius of the NFW-profile. Since the expected loss of subhaloes and galaxies due to tidal disruption increases the velocity dispersion of surviving galaxies, the observed galaxy velocity dispersion can substantially overestimate the virial mass.

Key words: galaxies:groups:general - cosmology:dark matter - methods:numerical

1 INTRODUCTION

Clusters of galaxies have been extensively studied in all available wave bands. They belong to the most massive and eye-catching structures in the Universe and are thought to closely resemble the cosmic composite of 85 per cent dark matter and 15 per cent baryonic matter (Spergel et al. 2006). According to the hierarchical model for structure assembly, these systems preferentially have formed late. For dark matter haloes it has been shown that the formation redshift is correlated with concentration (e.g. Bullock et al. 2001; Wechsler et al. 2002) therefore clusters present a class of low concentration objects. In contrast, groups of galaxies span a whole range of formation times and concentrations. Some resemble the properties of clusters (Zabludoff & Mulchaey 1998; Mulchaey 2000; Zabludoff & Mulchaey 2000), having low concentrations, others show an opposite behaviour.

Also the properties of the galaxy populations vary strongly amongst individual groups. Some groups have lumi-

osity functions similar to those observed in clusters but 'fossil groups' display a central giant elliptical galaxy with only few intermediate-luminosity galaxies (e.g. Ponman et al. 1994; Jones et al. 2003). The optical properties of the central bright galaxies are consistent with an origin as the merged combination of a more typical, less over-luminous, galaxies. The variations amongst the satellite populations are thought to originate from varying formation times. Using N-body experiments D'Onghia et al. (2005) demonstrated that the earliest formed group-sized dark matter haloes reveal structural similarity to observed fossil groups (see also Sommer-Larsen 2006). The early formation times of fossil groups also impacts satellite galaxies that do not merge with the central giant. Based on the observed depletion of intermediate-luminosity galaxies in the fossil group RX J1552.2+2013, Mendes de Oliveira et al. (2006) suggests that the members of this system may be affected by tidal disruption. Da Rocha & Mendes de Oliveira (2005) find substantial amount of intra-group light in two of three compact groups which may, at least partly, come from tidally

dissolved satellite galaxies. These observations indicate a substantial variation of the satellite population with time either by merging or by tidal dissolution.

In addition to the concentration-age and the luminosity-age relations, we describe here a concentration-velocity relation. According to the Jeans equation, galaxies orbiting in more concentrated host haloes have higher velocity dispersions. This effect is most pronounced in the central regions of the host halo. As discussed above, early formed groups are more concentrated, leading to the conclusion that the central satellite galaxies in fossil groups move faster than central galaxies in less evolved groups of comparable size. Additionally, if tidal disruption reduces the number of satellite galaxies, the velocity dispersion of the remaining galaxies is expected to increase even higher. The last statement is supported by the following consideration. Analysing N-body simulations, Diemand et al. (2004) find an enhanced velocity dispersion of subhaloes compared to the dispersion of the diffuse dark matter component. Subsequently, Faltenbacher & Diemand (2006) argued that the loss of a slow moving, earlier accreted, subset of the subhalo population is responsible for this bias. In analogy, if satellite galaxies are prone to tidal dissolution, then early accreted, slow moving, galaxies are preferentially dissolved. The lack of low velocity galaxies causes an enhanced velocity dispersion of the remaining galaxies. An observational hint for such a scenario may be the recent observation of the fossil system RX J1416.4+2315 by (Khosroshahi et al. 2006). Based on 18 member galaxies they find a velocity dispersion that is nearly twice as high as expected from the X-ray analysis of this system.

These findings motivated us to study the relation between the host concentration and dynamics of the subhalo populations. The paper is organised as follows. § 2 introduces the dynamical model used to trace the evolution of substructure in host haloes of different mass accretion histories. § 3 deals with substructure as point-like particles, a reference for the subsequent more complex investigation. § 4 presents dynamical results when substructures are treated as extended units prone to tidal stripping and dynamical friction. Finally, § 5 concludes with a summary.

2 DYNAMICAL MODEL

We aim to investigate the correlation between the host concentration and subhalo dynamics. In principle cosmological N-body simulations can best tackle these kinds of problems. However, such simulations should cover a large volume for satisfactory host halo statistics and, at the same time, provide high resolution for the accurate determination of the subhalo dynamics. Here we pursue an alternative approach. We employ semi-analytical models to gain a basic understanding of the processes which shape the subhalo distributions within equal mass hosts of various concentrations.

In recent years high resolution CDM simulations have substantially improved our understanding of cosmic structure formation. This insight can be used to model the dynamical evolution of subhalo in a semi-analytical manner. Recently, Zentner et al. (2005) demonstrated that this kind of semi-analytical modelling achieves good agree-

ment with state of the art N-body simulations. Similar approaches have been used for a variety of scientific goals (see e.g. Bullock et al. 2000, 2001; Zentner & Bullock 2003; Koushiappas et al. 2004; Taylor & Babul 2001, 2004; Islam et al. 2003; van den Bosch et al. 2005).

Here we extend the models presented in Mathews et al. (2004) and Faltenbacher & Mathews (2005). Originally, these models were designed to reproduce the well observed number density distribution of satellite galaxies of the NGC 5044 group. These models have been modified for the purposes of present investigation. Basically, the model integrates the orbits of subhaloes from the accretion onto the host to the present ($z = 0$) within the deepening gravitational potential of the host halo. By means of this the origin of the present subhalo distribution can be investigated. Also, the code allows us to assign a mass profile to the entering subhaloes which in turn can be used to compute the modification of their orbits by tidal mass loss and dynamical friction.

2.1 Host halo

Based on the analysis of N-body simulations Wechsler et al. (2002) found that the mass growth of CDM haloes can be described by

$$M_v(a) = M_{v,0} e^{-2a_f (\frac{1}{a}-1)} \quad (1)$$

where $a = 1/(1+z)$ and $a_f = 1/(1+z_f)$ is the cosmic expansion factor at the formation redshift z_f . Given the present virial mass of a halo, the mass accretion history is fully determined by the only remaining free parameter a_f . Individual accretion histories may differ strongly from this description, but on average the mass accretion is well approximated by this formula. Most importantly, the mass built-up of a halo is separated into two distinct phases, namely an early rapid accretion phase and a subsequent period of modest accretion. Knowing $M_v(a)$ also allows to compute the evolution of the virial radius $R_{vir}(a)$. According to the spherical collapse model the virial radius $R_{vir}(a)$ is the radius which includes a mean density of $\Delta(a)\rho_c(a)$, where $\Delta(a)$ is the virial over-density in units of the critical density $\rho_c(a)$ (see e.g. Eke et al. 1998; Bryan & Norman 1998).

$$R_{vir} = \left(\frac{3M(a)}{4\pi \Delta(a)\rho_c(a)} \right)^{1/3} \quad (2)$$

Anticipating an NFW density profile (Navarro et al. 1997), the host mass and concentration are sufficient to completely determine its properties. According to Wechsler et al. (2002) the evolution of the concentration is given by

$$c_{vir} = \frac{c_1 a_0}{a_f} \quad (3)$$

where $c_1 = 5.125$ according to Zentner et al. (2005) and a_0 , the cosmic expansion factor at the time of observation, equals 1 in this context. In our model Eqs. 1 and 3 completely characterise the growth of the host and its gravitational potential which in turn determines the orbits of the subhaloes. At $z = 0$ all host haloes approach the same virial mass ($M_{v,0} = 3.9 \times 10^{13} M_\odot$), but they exhibit concentrations in the range between 2 and 20 (integer steps, resulting in 19 output sets). The low concentration haloes are currently in the rapid accretion phase. According to Eq. 3 the

formation of the least concentrated haloes takes place in future times. The most concentrated haloes formed at redshifts $z \sim 3$. The evolution of the host haloes as described here does not explicitly include merging events. Such events may rearrange the phase space distributions of the subhaloes. However, the rapid accretion phase at early times causes the fastest change of the potential over the whole accretion history of a halo. To a certain extent these violent merging processes are covered by the steep slope of the accretion (equation 1) at z_f .

In summary, the mass growth of the host haloes modelled according to Eq. 1 provides the background potential for the dynamical evolution of the subhaloes. All hosts have a mass of $M_{v,0} = 3.9 \times 10^{13} M_\odot$ at $z = 0$ and concentrations ranging from 2 to 20 (integer steps). According to Eq.3 concentrations are associated with formation times, resulting in different accretion histories for the host haloes despite their equal masses.

2.2 Subhaloes

After introducing the model for the host we now describe the host's substructure population. Two samples of 100000 orbits are traced for every host halo. The first sample, referred to as the *point mass sample*, follows the evolution of point-like particles within the potential of the host. In the second sample, dubbed the *subhaloe sample*, the orbits are modified by the effects of tidal stripping and dynamical friction which involve the attribution of density profiles to each substructure. The point mass sample is mainly used to test the agreement of the model with N-body simulations on a particle basis. The subhaloes in the subhaloe sample have masses $\gtrsim 5 \times 10^8 M_\odot$ which renders them possible candidates for hosting galaxies. Obviously, the sum of all 100000 subhaloe masses exceeds the mass of the host halo. Therefore, the results for the subhaloe distributions should be considered as the outcome of stacking many identical groups. In the next two paragraphs we describe the generation of the initial conditions and initial properties of the subhaloes in the subhaloe sample.

2.2.1 Orbital initial conditions

We assume that the initial space density of the subhaloes is proportional to the dark matter, i.e. subhaloes enter the host halo in proportion to the dark matter. To generate this particular accretion pattern the individual arrival times of the subhaloes are assigned by a random process using the mass of the host as a proxy for the cosmic time.

$$M_i = \mathcal{R}_A M_{v,0} \quad (4)$$

Here $0 \leq \mathcal{R}_A \leq 1$ is a random number and $M_{v,0}$ the virial mass of the host at $z = 0$. By setting $M_i = M(a)$ (Eq. 1) M_i can be converted into the cosmic expansion factor a_i or equivalently z_i , which is considered as the accretion time of the *ith* subhaloe. Subsequently Eq. 2 is used to derive virial radius of the host, r_i , at that time. The *ith* subhaloe is assumed to be gravitationally accelerated by M_i from standstill at the turnaround radius ($r_{turn} = 2r_i$) until it reaches the virial radius, r_i . The resulting absolute values of the

velocity at r_i is

$$u_i = (GM_i/r_i)^{1/2} \quad (5)$$

which also equals the circular velocity at r_i . To assign an angular momentum to each subhaloe we invoke another random process designed to reproduce the distribution of circularities found in N-body simulations. The circularity is defined as $\epsilon \equiv J/J_c$ where J is the angular momentum of the orbit and J_c is the angular momentum of a circular orbit with the same orbital energy (see e.g. Lacey & Cole 1993; Tormen 1997). Zentner et al. (2005) present the orbital circularity distribution for subhaloes in N-body simulations at the time of entering the virial radius of the host. They also provide a fitting formula for the distribution and state that it is independent of accretion redshift and subhaloe mass. Here we model the probability distribution of circularities with a simple quadratic, $dp/d\epsilon = 6\epsilon(1-\epsilon)$, which is in fairly good agreement with the data presented by Zentner et al. (2005) and has a mean circularity of $\langle \epsilon \rangle = 0.5$. The initial angular momentum of a subhaloe is randomly drawn from this distribution,

$$\mathcal{R}_L = \int_0^\epsilon 6\epsilon(1-\epsilon)d\epsilon = 3\epsilon^2 - 2\epsilon^3, \quad (6)$$

where \mathcal{R}_L is a random number between zero and one. Note, the distributions of circularities were derived for subhaloes in N-body simulations, here we implicitly assume that the same regularity holds for the point mass sample as well.

Knowing the evolution of the host potential, the accretion time and the initial orbital parameters of each subhaloe, the integration of the orbits can be pursued. Details about the integration are presented at the end of the following paragraph. Two random processes are involved to generate the orbital initial conditions, namely \mathcal{R}_A for the arrival time and \mathcal{R}_L for the initial angular momentum. We assume, that the orbital energy is uniquely determined by the host virial mass and radius at the time of arrival, which may not be exactly the case (see Zentner et al. 2005). However, for simplicity we do not implement an additional mechanism to spread the distribution of initial orbital energies.

2.2.2 Subhaloe properties

As long as the subhaloes are treated as point-like particles and dynamical friction is ignored, the orbits are independent of the subhaloe masses. For a more realistic model we must consider the spatial extension of the subhaloes and as a consequence the susceptibility to tidal truncation. For that purpose a mass is attributed to every arriving subhaloe by a random process which is set up to generate a power law mass function as observed for the field haloes in N-body simulations. We adopt $dM/dN = M^\alpha$ where $\alpha = -1.86$ (Somerville & Primack 1999; Reed et al. 2003). Consequently, the mass of the *ith* halo m_i at arrival is given by

$$m_i = [M_1^x - \mathcal{R}_M(M_1^x - M_2^x)]^{1/x} \quad (7)$$

where \mathcal{R}_M is a random number between 0 and 1, $x = 1 + \alpha$. The lower mass limit is $M_1 = 5 \times 10^8 M_\odot$ and the upper mass limit is $M_2 = M_i$, where M_i is the current host mass (see Eq.4). We only focus on the evolution of dark matter haloes above $M_1 = 5 \times 10^8 M_\odot$ because they are massive enough to

potentially host visible galaxies. The upper mass limit is chosen to avoid merging of haloes more massive than the current host. Note, since the mass function is so steep our results do not depend on the exact choice of the upper mass limit. This restriction assures that we follow the host merging tree along the most massive progenitors. Ignoring the possible deviations caused by the centrally condensed baryonic matter, we associate an NFW density profile (Navarro et al. 1997) to every arriving subhaloe. We assume that the formation redshift of all (sub)haloes is $z_{sub,f} = 7$ (which corresponds to $a_{sub,f} = 0.125$). By setting the arrival time $a_i = a_0$ in Eq. 3 the concentration c_i of the subhaloe is computed. The density profile of the subhaloe is completely determined by m_i and c_i . We assume that on the subsequent orbits the shape of the density profile does not change (see Kazantzidis et al. 2004) however it can be truncated due to tidal forces. The tidal truncation radius is estimated by the Jacobi limit (see Binney & Tremaine 1987; Hayashi et al. 2004),

$$r_J = \left(\frac{m_{c,i}}{3M(< D)} \right)^{1/3} D \quad (8)$$

Here D is the instantaneous distance of the subhaloe from the centre of the host, $M(< D)$ is the host mass within D and $m_{c,i}$ is the current mass of the subhaloe. If r_J is smaller than the current radius of the subhaloe, all the matter outside of r_J is assumed to be stripped instantaneously and the current halo radius is replaced within r_J .

The orbits of the subhaloes are found by solving

$$\frac{d\mathbf{r}}{dt} = \mathbf{u} \quad \text{and} \quad \frac{d\mathbf{u}}{dt} = -\frac{GM(r)\mathbf{r}}{r^2} + \left(\frac{d\mathbf{u}}{dt} \right)_{df} \quad (9)$$

where $M(r)$ is the NFW mass within radius r of the host. Orbits are computed from redshift z_i (redshift at arrival) to the present epoch, $z = 0$. For the integration we use a fourth order Runge-Kutta integration scheme with adaptive time stepping.

The deceleration by dynamical friction (Chandrasekhar 1943; Colpi et al. 1999) is described by

$$\left(\frac{d\mathbf{u}}{dt} \right)_{df} = -\mathbf{u} 4\pi \ln \Lambda G^2 m \rho u^{-3} [\text{erf}(X) - \frac{2}{\pi^{1/2}} X e^{-X^2}]. \quad (10)$$

Here $\rho(r, t)$ is the local density of the host halo, $u = |\mathbf{u}|$ is the velocity of the subhaloe, $X = u/(\sqrt{2}\sigma)$ and $\sigma(r, t)$ is the mean velocity dispersion of diffuse dark matter in the host halo. We assume that the total dispersion can be approximated by the cold dark matter dispersion presented by Hoefl et al. (2004) (see also Mathews et al. 2004). We choose $\ln \Lambda = 3$ as suggested by Zhang et al. (2002) which is the point mass approximation. This approximation is justified by the very efficient tidal mass stripping which rapidly truncates the radius of the subhaloe to a few per cent of the virial radius of the host.

In summary, a mass is randomly assigned to each arriving subhaloe. The random process is designed to recover the mass functions of field haloes found in N-body simulations. Additionally a concentration is assigned to the subhaloe assuming a common (sub)haloe formation redshift of $z = 7$. Based on mass and concentration an NFW density profile is associated with each subhaloe. The profile is assumed to maintain its shape on the subsequent orbit within the host potential well, however tidal truncation is allowed

to take place. The subhaloe gets most severely truncated at its peri-centre passage. The remaining mass remains constant until the subhaloe approaches the centre for the next time. Between two subsequent peri-centre passages the subhaloe loses some orbital energy due to dynamical friction, the peri-centre distance shrinks with each passage, reducing the truncation radius. Of course, lower masses experience less dynamical friction. The mass of the subhaloes decreases in a step-like fashion, as also observed in N-body simulations (e.g. Kravtsov et al. 2004; Boylan-Kolchin & Ma 2006).

In order to investigate how tidal reduction affects the properties of the subhaloe population we will construct a sub-subhaloe sample containing only subhaloes having present truncation radii above the *rejection* radius $r_{rej} \gtrsim 3$ kpc. This choice is somewhat arbitrary, but in agreement with values given in Faltenbacher & Mathews (2005) who achieve good agreement between the outcome of a very similar dynamical model for the observed galaxy group NGC 5044. Subsequently, we refer to the two subsamples as then *complete* and *reduced* samples, emphasising that the latter is a subset of the former. Note, disappearance when $r \leq r_{rej}$ in the reduced subhaloe sample does not necessarily mean total physical disassembly of the object, it may just mean that it falls below a given detection limit. Such limits are apparent in both simulations and observations. The detection of subhaloes in simulations is constricted by a minimum particle number limit for substructures and the detection of satellite galaxies in groups depends on the sensitivity of the observations.

3 RESULTS FOR THE POINT MASS SAMPLE

The point mass sample follows the evolution of point-like particles within the growing potential well of equal-mass host haloes with varying accretion histories. Mass dependent mechanisms, like tides and dynamical friction, are excluded. The mass of the particles is irrelevant. In this section we (1) demonstrate the agreement of the model with established results from N-body simulations and (2) discuss the concentration-sigma relation for this simplified approach as a reference for the results for the (complete and reduced) subhaloe samples presented in the following section.

3.1 Accretion histories

The particles, or later subhaloes, enter the host halo in proportion to the dark matter. The growth of the dark matter host halo is described by Eq. 1. The generation of the initial condition for each particle includes two random selections, the arrival time and the initial angular momentum. After the first penetration of the host virial radius the orbits are integrated numerically. Fig. 1 displays the expansion factor at accretion time versus the current particle distance from the centre the host, showing distributions for host concentrations of 6, 10 and 20. Subsequently, whenever properties of individual hosts shall be exemplified we use these tree concentrations and refer to the accordingly, as the c_6 , c_{10} and c_{20} hosts. Despite the angular momentum distribution imposed on the particles, caustic-like features are apparent as discussed in the context of the secondary infall model by Bertschinger (1985). The most prominent feature is caused

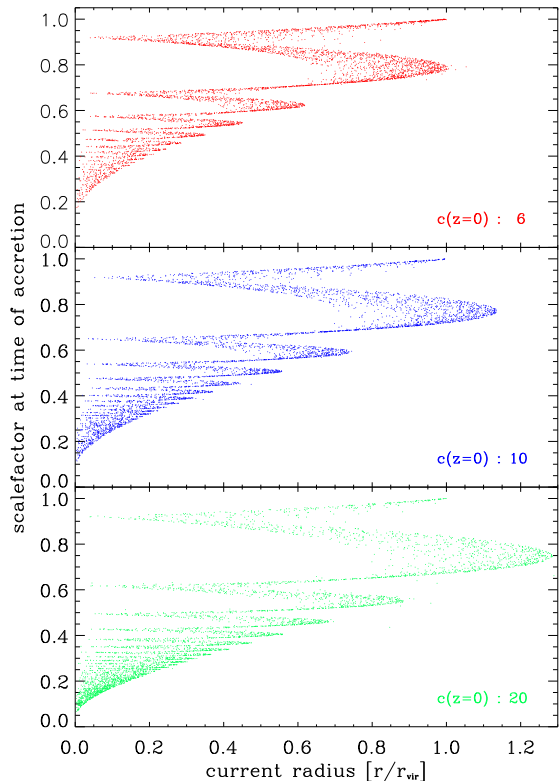


Figure 1. Scale factor at time of accretion versus current subhalo distance to the centre for the three example host halo concentrations of 6, 10 and 20 at $z = 0$. For clarity, only 5 per cent of the 100000 particles, randomly selected from the complete samples, are displayed. Even if weakened due to the imposed angular momentum distribution, there is a clear indication for the appearance of caustics as described in secondary infall model by Bertschinger (1985). The caustic of the second turnaround is located at or beyond the current virial radius. The caustic of the most concentrated host extends furthest, indicating the highest orbital energies.

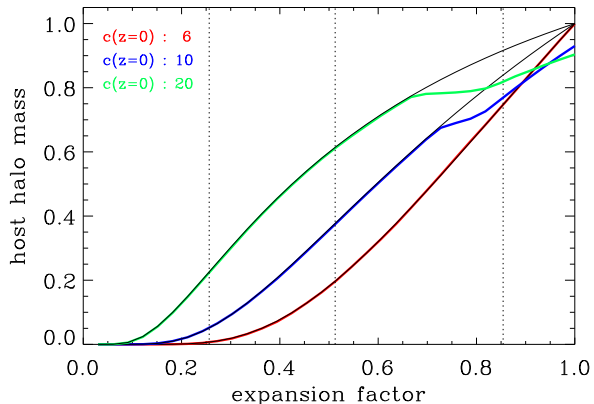


Figure 2. Accretion histories for three host halo concentrations at $z = 0$ compared to the analytical description in Wechsler & al. (2002), thin solid lines. The negative deviation from the Wechsler formula at late times results from the loss of particles in of the secondary caustic that extends beyond the current virial radius, see Fig. 1.

by the *caustic of the second turnaround* generated by the particles when they reach the apo-centre after their first peri-centre passage. Investigating the dynamics of the NGC 5846 group Mahdavi et al. (2005) find observational support for the appearance of the caustic of the second turnaround. The location of the second caustic is correlated with the host concentration. For the c_6 host the caustic is located at the virial radius whereas in the c_{20} host it is found at ~ 1.3 times the virial radius. For all host concentrations, the second turnaround is experienced by particles accreted at $a \sim 0.8$.

Fig. 2 compares the mass growth of the host halo (thin solid lines) to the particle accretion history for all particles located within the host virial radius at $z = 0$ (three heavier lines). Both quantities, host mass and particle numbers, are normalised to unity. The deviations at late times are caused by particles with orbits currently beyond the virial radius also seen in Fig. 1.

The positive correlation between the group-centric distances of the caustics and the concentrations in Fig. 1 arises from the more rapid mass assembly of high concentration hosts. The thin solid lines of Fig. 2 indicate that at $a = 0.8$. The c_{20} host has already assembled 90 per cent of the final mass compared to only 60 per cent for the c_6 host. Thus at the time ($a \sim 0.8$) when the particles are accreted that presently pass through the second turnaround the c_{20} host is a factor of 1.5 more massive than the c_6 host. Therefore its virial radius is larger by a factor of $1.5^{1/3} = 1.14$. However, Fig. 1 shows a factor of ~ 1.3 difference between the location of the c_{20} and the c_6 turnaround. This additional shrinking of the second turnaround radius within the less concentrated host is caused by the rapid mass growth of the c_6 host at the present time. Thus particles moving outward after their first peri-centre passage feel a much deeper potential well, which prevents them from reaching their original starting point, the first turnaround when they decouple from cosmic expansion. In contrast, the highly concentrated hosts don't show such a rapid deepening of its potential at late times, so the particles can move further out.

3.2 Density profiles

The host mass grows according to Eq. 1 and the evolution of the concentration is given by Eq. 3. The rate that particles (the same applies to subhaloes) enter the virial radius of the host is given by Eq. 7. About half of all the particles are accreted onto the host before $z = 0.6$. Of course this value varies depending on the accretion histories which in our model are determined by the current concentration of the host. Fig. 3 compares the number density profiles for the three concentrations ($c = 6, 10, 20$) with NFW-profiles. The agreement of the analytical profiles with the results of the dynamical evolution is remarkable. The successful reproduction of the analytical profile by the dynamically evolved particle distribution provides strong evidence for the capability of the present model. There appear small deviations at the centre for the more concentrated hosts which may be caused by a lack of numerical resolution or by a slight inaccuracy of the employed accretion formula at early times (see Tasitsiomi et al. 2004; Zhao et al. 2003). However, this occurs only within a few per cent of the virial radius and will not affect the results presented here.

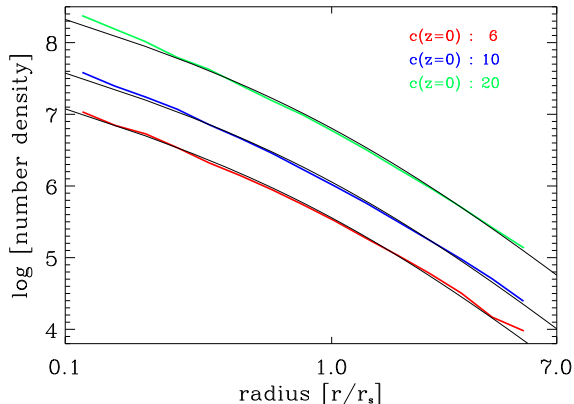


Figure 3. Arbitrarily scaled number density profiles of the particles for three host concentrations. The thin solid lines display the NFW-profiles for the corresponding concentrations. The group-centric distances are scaled by r_s , the characteristic radius of the NFW-profile ($r_s = R_{vir}/c$).

3.3 Velocity dispersion profiles

We now focus on the velocity profiles of the point mass sample. In particular we derive a general expression for the anisotropy parameter $\beta = 1 - (\sigma_{t,1}/\sigma_r)^2$ where σ_r is the radial velocity dispersion and $\sigma_{t,1}$ is the uni-dimensional tangential velocity dispersion. If the tangential velocities are isotropic $\sigma_{t,1} = \sigma_t/\sqrt{2}$, where σ_t is the two dimensional tangential velocity dispersion. By scaling the host-centric distances by r_s , the characteristic radius of the NFW-profiles, one achieves coincidence of the β -profiles independent of the concentration.

The upper panels in Fig. 4 display the radial mean velocities and the velocity dispersions of the particles for the three example hosts ($c = 6, 10, 20$). Negative values in the first panel indicate net infall. For the more concentrated hosts the radial velocities are close to zero, indicating fairly relaxed systems. The particles within the c_6 host show some slight net infall at $\sim 7r_s$ which may be a result of the recent rapid growth phase of the host halo. The velocity dispersions in the second panel show a behaviour known from N-body simulations (Hoeft et al. 2004), they peak at about $0.8r_s$. In the third panel the velocity dispersions are split up into radial and tangential components. To allow for a direct comparison with the radial component the uni-dimensional tangential velocity dispersion $\sigma_{t,1}$ is shown here. Finally, the anisotropy profiles $\beta(r/r_s)$ for the three host haloes are given in the lowest panel. Despite the different host concentrations, we find that the anisotropy profiles are very similar if the distances are scaled by the characteristic radius r_s of the NFW-profile rather than the virial radius R_{vir} . The β -profiles can be fit with an concentration-independent expression:

$$\beta(r) = b \left(\frac{x}{x+1} \right)^a \quad x = r/r_s \quad (11)$$

This expression enables an analytical integration of the Jeans equations as discussed in the Appendix.

In addition to the successful reproduction of the density profiles the present inspection of the velocity profiles confirms that the dynamical properties of our model are

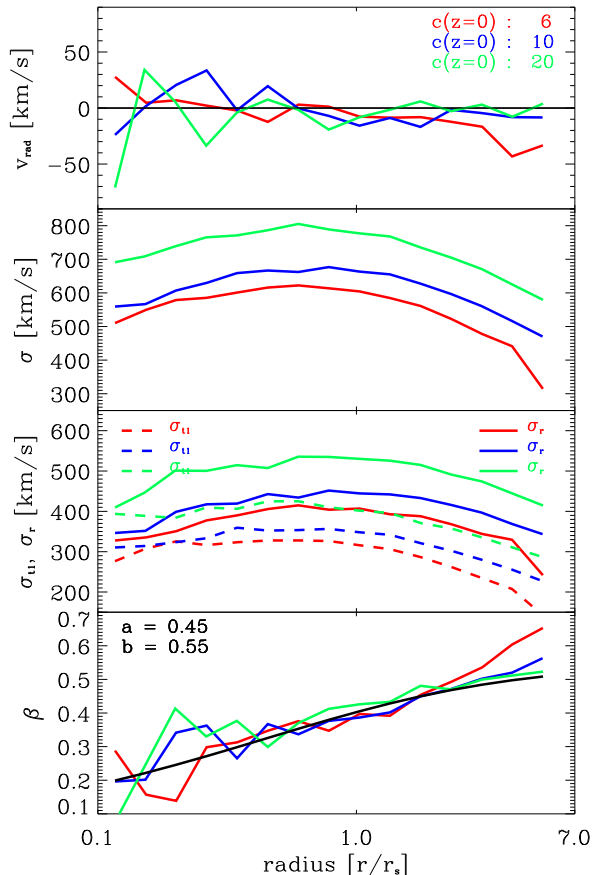


Figure 4. The upper three panels display mean radial velocity (v_{rad}), the velocity dispersion (σ) and the orthogonal velocity dispersion components (radial σ_r and 1D tangential $\sigma_{t,1}$) of the particles within host haloes of three concentrations. The group-centric distances are scaled by r_s , the characteristic radius of the NFW-profiles ($r_s = R_{vir}/c$). Negative values for the mean velocities in the first panel indicate net infall. The lowest panel shows the associated anisotropy profiles $\beta(r)$. The black solid line displays the β -fit given in Eq.11, with an exponent of $a = 0.45$ and a scaling $b = 0.55$. Note, the anisotropy profiles of different concentrations can be fitted equally well with the same parameters.

also in good agreement with the dynamical characteristics of CDM haloes generated by N-body experiments. Based on 10 relaxed dark matter halos Wojtak et al. (2005) find a similar shape and asymptotic values for the average β -profile. Also the β -profiles based on six highly resolved N-body systems presented by Dehnen & McLaughlin (2005) (based on simulations discussed in Diemand et al. (2004) and Diemand et al. (2004a)) show very similar features. Finally, the density slope - velocity anisotropy relation discussed in Hansen & Moore (2006) implies a self similarity of β -profiles when scaled by r_s as advocated here.

3.4 Concentration-sigma relation

We now investigate the relation between the mean particle velocity dispersion and the concentration of the host haloes. It is expected that the velocity dispersion increases with concentration, therefore the present results should be con-

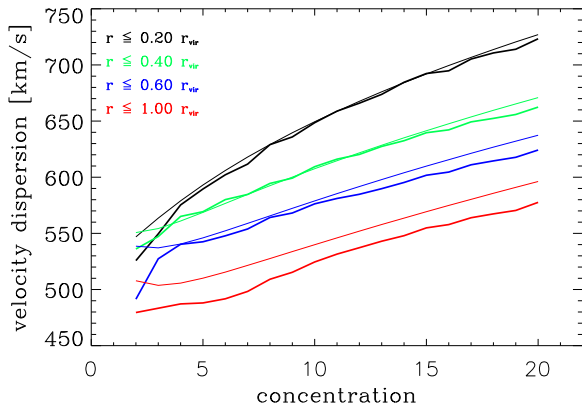


Figure 5. Mean velocity dispersions within the listed fractions of the virial radius versus the host concentration. The thick lines display the results from the dynamical models and the thin solid lines arise from the numerical integration of the Jeans equation using the β -formula Eq. 11 (see Appendix).

sidered as an further affirmation of the model and a point of reference for subsequent investigations of the subhaloes sample.

Fig. 5 shows the dependence of the mean particle velocity dispersions on the host concentrations. The mean values of the dispersions are computed within several fractions of the virial radius. The thin solid lines display the results from the analytical integration of the Jeans equation using Eq. 11 to describe the radial behaviour of the anisotropy parameter. Details of this integration can be found in the Appendix. The agreement between the model and the analytical computation is convincing. For very small concentrations $\lesssim 5$ some deviations appear, but hosts haloes with these small concentrations are in the process of formation and the applicability of the Jeans equation in this form may be questioned. The ~ 5 per cent deviation for the mean dispersion within the full virial radius $1.00R_{vir}$ probably results from the orderly accretion mode inherent in our model. Its traces are certainly not blurred out before the second turnaround passage (see also Fig. 1). The main finding is that the velocity dispersion for hosts with concentrations ~ 20 are a factor of 1.2–1.3 higher than the mean velocity dispersions of equal mass hosts with concentrations ~ 5 . The mean central velocity dispersions increase somewhat stronger with the host concentration than those within larger radii.

In summary, our comprehensive examinations of the point mass sample have shown satisfactory agreement with the results from N-body simulations, indicating that our simplified dynamical model can reproduce the main characteristics found by more elaborate N-body simulations. However, we notice that the outskirts ($\gtrsim 0.6R_{vir}$) may be slightly affected by the unphysical regularity of the accretion mode. Nevertheless, the model enables us to measure in detail the dependence of the subhaloe properties on the host concentration.

4 RESULTS FOR THE SUBHALOE SAMPLES

This section describes the dynamical evolution of extended subhaloes within the growing potentials of their hosts. As described in § 2.2.2 we attribute to every (sub)haloe a NFW-density profile and include the effects of dynamical friction and tidal truncation in the integration of the orbits. For every host we distinguish two subhaloe samples at $z = 0$, a *complete* sample and a *tidally reduced* sample. The former comprises all 100000 subhaloes independently of their present truncation radius and the latter counts only those subhaloes whose tidal truncation radius is larger than 3 kpc. The tidally reduced sample is a sub-sample of the complete sample. For example, the reduced samples of the c_6 , c_{10} and c_{20} host haloes comprise a number of 74777, 57218, 36258 surviving subhaloes, respectively, of the original 100000 within the complete sample. The idea behind this distinction is to imitate the effects of detection limits which are inherent to observation and simulations. If satellite galaxies fall below a certain luminosity, they won't appear in the catalogue. And if subhaloes fall below a certain particle limit they won't be counted as substructure. In both cases the disappearance from the catalogue does not necessarily mean total physical disassembly. The accretion times and the assembly history of the subhaloes samples do not differ from those plotted in Figs. 1 and 2) for the point mass sample. Consequently, we start the investigation of the subhaloe samples with the discussion of the evolution of the mass function.

4.1 Mass functions

The assignment of initial subhaloe masses is designed to reproduce a differential mass distribution dN/dM with a power law shape and a logarithmic slope of $\alpha = -1.86$, the appropriate slope for field haloes measured in N-body simulations. The upper panel of Fig. 6 compares the differential mass functions of the arriving subhaloes (thin lines) with the mass function of the complete subhaloes at $z = 0$ after they were dynamically processed within the three example hosts ($c = 6, 10, 20$). The mass functions are shown within a range of $5 \times 10^8 - 2 \times 10^{12} M_\odot$. The initial mass functions for the three concentrations perfectly coincide, indicating that the temporarily slightly different upper mass limits due to the altering host growth rates (see Eq. 7) do not affect the overall mass function. Interestingly the logarithmic slope does not change for the dynamically processed subhaloe samples at $z = 0$. Similar results have been found in N-body simulations (e.g. Reed et al. 2005). There appears a slight dependence of the amplitude of the dynamically processed mass functions on the host concentrations. More concentrated hosts have slightly reduced mass functions. The reason for the weak dependence on host concentration can be explained by the correlation between mean subhaloe accretion times and host concentrations as displayed in Fig. 7. On average subhaloes in more concentrated hosts are accreted earlier, thus they are exposed to the tidal field of the host for a longer time and they suffer more severe mass losses. The thick lines in the lower panel of Fig. 6 may clarify this issue. They display the ratios of initial to the final subhaloe mass function. The c_6 host exhibits a difference in amplitude of a factor of ~ 2 , whereas in the c_{20} host the final mass function is reduced by

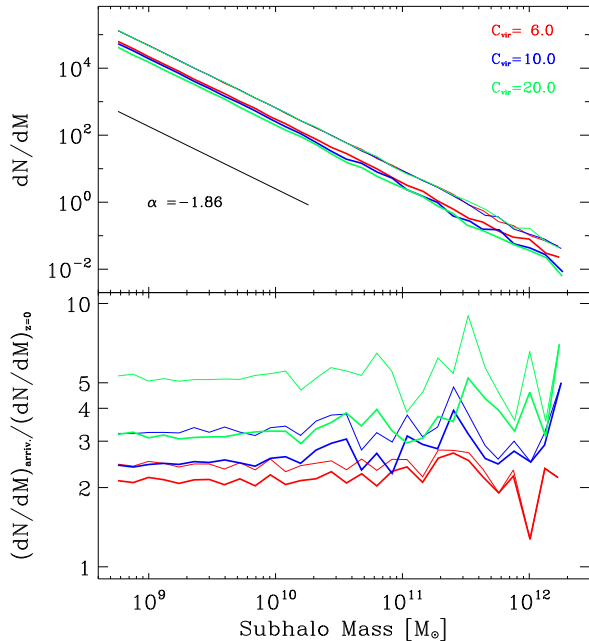


Figure 6. The upper panel compares the differential mass function of the subhaloes in the complete sample before entering the virial radius of the host (thin lines) with the mass function of the subhaloes at $z = 0$ (thick lines). The straight line displays the slope used in Eq. 7. There is a weak dependence of the amplitude of the final mass function on the concentration. The lower panel shows the ratios of the initial to the present mass functions. Thick lines are used for the complete subhalo sample (these values can be directly read off the upper panel). The thin lines in the lower panel display the ratios between the mass function of the initial subhalo mass function to the tidally reduced sample.

a factor of ~ 3 . The thin lines in the lower panel display the ratios between the initial and the final mass distributions in the tidally reduced subhalo sample. At the low mass end the difference between initial and final mass function is enhanced, however the high mass end shows barely any difference. Therefore, at the low mass end the power law slope is conserved even in the tidally reduced sample. The solid line in Fig. 7 displays the mean accretion times as a function of host concentration for the tidally reduced sample. In particular for concentrations ~ 20 the difference of the mean accretion time is about 3.5 Gyr.

4.2 Density profiles

Fig. 8 shows the number density profiles for the complete and the tidally reduced subhalo samples within the three host haloes with present concentrations of 6, 10 and 20. In contrast to the density profiles in Fig. 3 the distances from the centre of the host are scaled by the virial radius R_{vir} . For comparison the associated NFW-profiles are displayed with thin solid lines. Similar to findings for the point mass sample in § 3.2, the agreement between the NFW-profile and the complete sample is remarkable, indicating that the combined action of dynamical friction and tidal truncation does not severely alter the number density profile. Subhaloes lose a substantial fraction of their mass during their first peri-

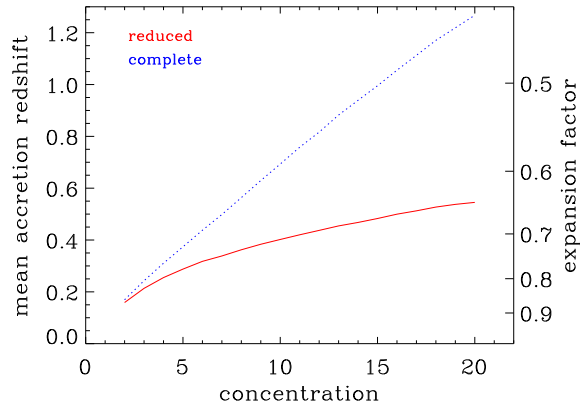


Figure 7. Variation of mean accretion redshift of subhaloes with host concentration at $z = 0$. The dotted line shows the results for the complete subhalo sample. The solid line displays the relation for the tidally reduced subhalo sample.

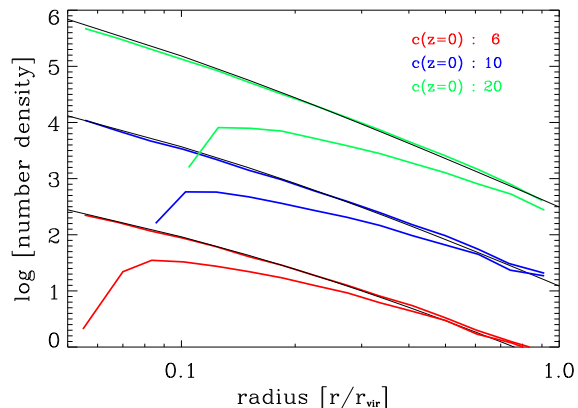


Figure 8. Arbitrarily scaled number density profiles for the complete and the tidally reduced subhalo sample within host haloes of three concentrations ($c=6, 10, 20$). The thin solid lines give the associated NFW-profiles. The complete sample shows perfect agreement with the NFW-profiles. The profiles of the tidally reduced samples flatten towards the centre. Subhalo populations in more concentrated hosts are more efficiently reduced.

centre passage, after that the dynamical friction is strongly reduced since dynamical friction drag is proportional to the subhalo mass (Eq. 10). The number densities of all tidally reduced samples show a centrally flattened behaviour, indeed at the very centre they display positive gradients. We do not discuss to what extent these positive gradients are physical since the presence of baryons in subhaloes certainly alters their tidal resistance. However, it is noteworthy that most of tidal reduction within the c_6 host is confined to the volume within half the virial radius whereas the tidal reduction is visible over the whole halo volume in the case of the c_{20} host.

4.3 Velocity dispersion profiles

Some very interesting insights into the dynamics of subhaloes can be gained by comparisons of the velocity dis-

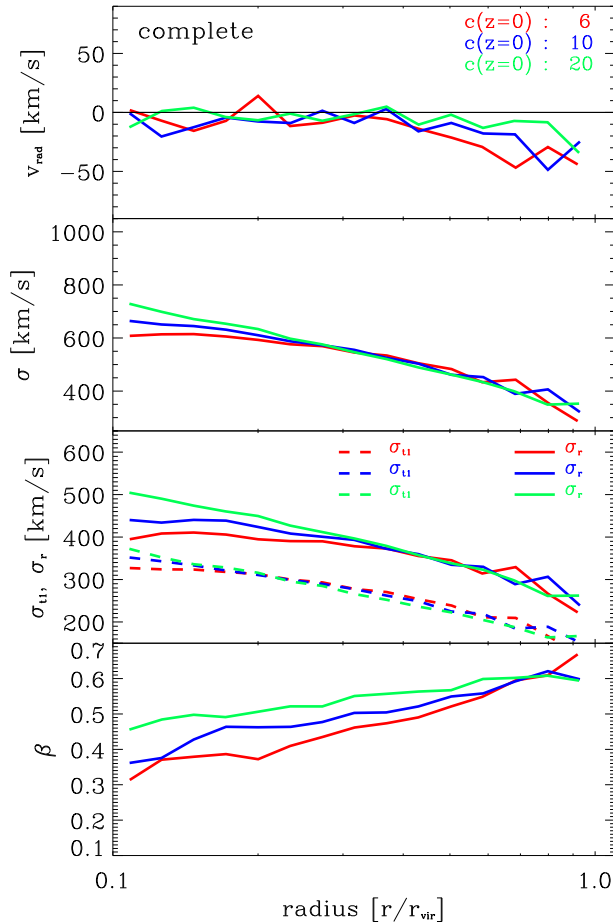


Figure 9. The upper three panels display mean radial velocity (v_{rad}), the velocity dispersion (σ) and the orthogonal velocity dispersion components (radial σ_r and 1D tangential $\sigma_{t,1}$) of the complete subhalo population within host haloes of the indicated concentrations. As distinct from Fig. 4, here the group-centric distances are scaled by virial radius R_{vir} .

tributions for the complete and the tidally reduced samples displayed in Figs. 9 and 10 respectively. It is important to keep in mind that the tidally reduced sample is a subsample of the complete sample. Therefore, higher mean velocities in the reduced sample can only be achieved if preferentially slow moving haloes are removed. In other words there is no source of high velocity haloes in the reduced sample. The uppermost panel in Fig. 9 displays the mean radial velocity of the complete sample. With exception of the outskirts they are close to zero, indicating a relaxed state. On the other side the mean velocities of the tidally reduced samples (Fig. 10) show a clear trend for inward motion, negative v_{rad} . This is most naturally explained by tidal shrinkage as subhaloes first approach the host centre. Consequently, most probably the truncation radii falls below the rejection radius of 3 kpc close to the peri-centre passage of the subhaloe, resulting in a lack of outward streaming subhaloes in the reduced sample. For large radii the velocity dispersions of the two samples are similar (second panels in Figs. 9 and 10). However, the central velocity dispersions of the reduced sample are ~ 1.3 times larger than in the complete sample. Again this increase

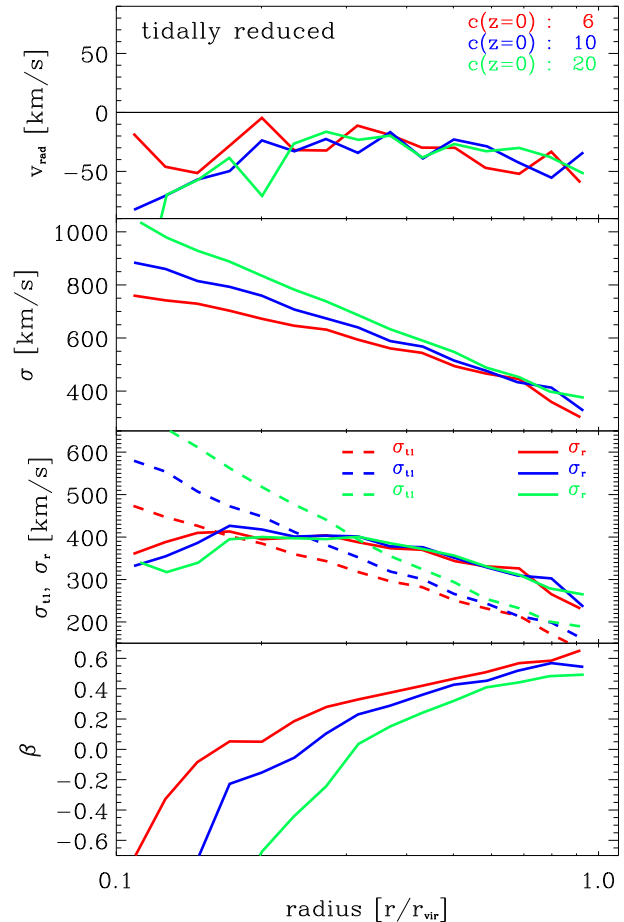


Figure 10. The upper three panels display mean radial velocity (v_{rad}), the velocity dispersion (σ) and the orthogonal velocity dispersion components (radial σ_r and 1D tangential $\sigma_{t,1}$) of the tidally reduced subhalo population within host haloes of the indicated concentrations. As distinct from Fig. 4, here the group-centric distances are scaled by virial radius R_{vir} .

of the velocity dispersion can only be explained by the lack of preferentially slow moving subhaloes. The comparison of the orthogonal components of the velocity dispersions (third panel in Figs. 9 and 10) indicates that the increase of the central velocity dispersion in the reduced sample is based on the strong enhancement of the tangential dispersions, which again must arise due to a lack of slow tangential motions. The radial components give the reverse picture. The central radial velocity dispersion of the reduced sample is actually smaller, indicating a deficit of fast radially moving subhaloes compared to the complete sample. A hint for this mechanism was reported by Faltenbacher et al. (2005) investigating the velocity distribution of galaxies in hydro-dynamical simulations of clusters of galaxies. The resulting anisotropy profiles are quite different (note the different scaling in the lowest panels of Figs. 9 and 10). If one assumes similar processes operating for satellite galaxy populations in simulated groups, the negative values for β displayed in Benatov et al. (2006) (their Fig. 5) are in agreement with the findings presented here. Macciò et al. (2006) discussed the enhanced survival rate of subhaloes with condensed baryonic cores. In theory

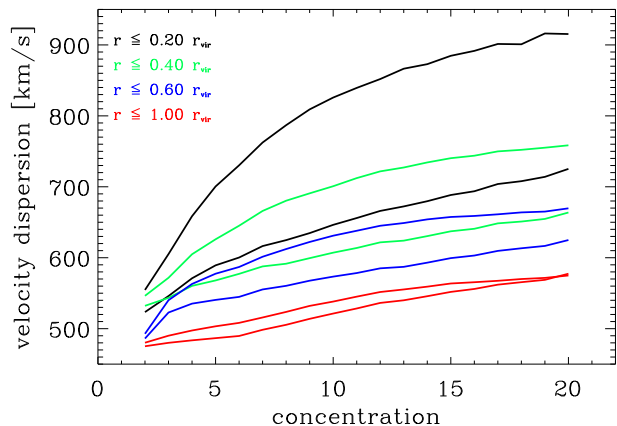


Figure 11. Variation of mean subhalo velocity dispersions with concentration of the host for various inclusion radii as listed. The upper line of each pair of lines with the same line style always displays the dispersion of the tidally reduced sample. The lower lines show the values belonging to the complete sample.

the behaviour of the velocity distribution of satellite galaxies in groups can be used to determine their tidal disruption rate.

4.4 Concentration-sigma relation

In analogy to Fig.5 we display in Fig.11 the mean dispersions within 0.2, 0.4, 0.6 and 1 times the virial radius R_{vir} for the complete and the tidally reduced subhalo samples. The larger dispersions always correspond to the tidally reduced sample whereas the lower line of each pair refers to the complete sample. The dispersions of the point mass sample in Fig.5 are quite similar to the values of the complete sample, indicating only a weak impact of dynamical friction on the global properties of the subhalo population. However, the impact of tidal reduction is enormous for the central dispersions, e.g. for host concentrations of ~ 20 the velocity dispersions within $0.2R_{vir}$ are enhanced by a factor of 1.3 compared to the complete sample. The dependence on concentration within the tidally reduced sample is also more prominent, the central dispersion in hosts with concentration ~ 5 to hosts with concentration ~ 20 increases by a factor 1.4. The mean dispersion within the virial radius is only weakly affected by the tidal reduction.

Since the complete sample resembles the behaviour of the point mass sample, the Jeans equation holds also in this case. Due to the negative mean radial velocities in the reduced sample (Fig. 11) one of the preconditions for the description by the Jeans equation is no longer valid (see Appendix). We do not aim to present a modified solution which can cope with radial motions, because the extent of inflow depends on the choice of the rejection radius in our model.

The important result here is that an increase in central velocity dispersion of satellite galaxies in groups caused by higher concentration may be amplified if some fraction of the satellite population has been tidally disrupted. Both trends are in the same direction. Low concentration hosts have relatively low central velocity dispersions and their recent formation times make tidal disruption as a driver for

an enhanced velocity dispersions unlikely. Strongly concentrated hosts have higher velocity dispersions and accreted most of their satellites early on. This old population may be more severely reduced by tidal forces, causing an additional boost to the central velocity dispersion.

5 SUMMARY

Using a dynamical model for the evolution of subhaloes within a growing host potential in galaxy groups, we have investigated the relation between host concentration and properties of subhalo population at $z = 0$. The concentration is correlated with the group formation redshift. Groups with equal virial masses at $z = 0$ but different formation times show significant differences in their subhalo properties. As a base point we have computed the dynamical evolution of point mass samples and their dependence on the host concentration. The model then has been adapted to cope with the spatial extent of subhaloes and the impact of dynamical friction and tidal disruption. We only focus on the dynamical evolution of subhaloes that are massive enough to possibly host galaxies. Every substructure analysis is subject to detection limits whether it is the sensitivity limit in connection with observations or the resolution limit in numerical simulations. To study the effects of detection limits, we create a *reduced* subhalo sample comprising only those subhaloes with current radii larger than a rejection radius of $r_{rej} = 3$ kpc. The reduced sample is a sub-sample of the *complete* sample, comprising all subhaloes independent of the actual truncation radius. The rejection radius can be considered as a parameter of the model and has been calibrated by observations as well as numerical simulations (see Faltenbacher & Mathews 2005). Originally the model is set up to trace the evolution of the dark matter subhaloes in a group environment, however if the subhaloes host luminous galaxies, a tidal truncation below 3 kpc most probably would affect the stellar component of the galaxy as well.

Our main findings are: (1) The velocity dispersion of subhaloes or satellite galaxies in groups depends on the concentration of the underlying dark matter distribution of the host halo. Equal mass hosts with higher concentrations have enhanced velocity dispersions of the subhaloes, in particular at the centre. Since higher host concentrations are caused by earlier formation times, this relation implies that subhalo populations with early formed hosts exhibit higher velocity dispersions than those residing in more recently formed hosts of equal mass. (2) We propose a fitting formula for the radial dependence of the anisotropy parameter β , which is independent of concentration if the group-centric distances when scaled by the characteristic radius of the NFW-profile r_s . (3) The increase of the central velocity dispersion with concentration is amplified in the reduced sample. This is caused by an enhancement of the tangential velocity dispersion and a lack of slow radial motions compared to the complete sample. (4) The dynamical evolution of subhaloes that experience tidal stripping and dynamical friction does not alter the slope of the mass function, in agreement with the results from N-body simulations (see e.g. Reed et al. 2005), but dynamical evolution reduces the amplitude by a factor of ~ 2 . In the complete sample the amplitude of the mass function is only weakly dependent

upon the host concentration. However, the reduced sample shows a stronger dependence on host concentration with amplitudes decreasing with increasing host concentrations. For a host concentration of 20 the amplitude of the initial mass function decreases by a factor of ~ 5 , however this value depends strongly on the choice of the rejection radius.

The present investigation reveals the difficulties associated with mass estimates derived from the velocity dispersion of satellites in groups. The concentration of the host haloes and the effects of tidal reduction of the satellite galaxies in groups may alter the central velocity dispersions. The appearance of intra-group stars is strong evidence for the reduction of the satellite luminosities. According to Osmond & Ponman (2004) the velocity dispersion provides a very unreliable measure of system mass. The concentration and its influence on tidal reduction add more concerns on the accuracy of such mass estimates.

Combined observations of X-ray temperatures and velocity dispersions of satellite galaxies have recently become available for groups. As an application of the present analysis these observations may be used to infer the impact of tidal forces onto the central satellite population. If tidal forces in fossil groups efficiently reduce the number of detectable satellites, we expect the central velocity dispersion to be high compared to the X-ray temperature. Some support for this scenario has been found by Khosroshahi et al. (2006).

A comparison of the X-ray temperatures of the hot intra-group gas with the velocity dispersions found for the satellite galaxies can be used to infer the degree of tidal disruption. A flattening of the central number density profiles along with an increasing velocity dispersion are the signatures of tidal reduction of the central subhalo or satellite population.

Sommer-Larsen (2006) considers radial velocity dispersions in fossil systems at a fixed radius $r \gtrsim 30$ kpc. We have presented a uniform fitting formula for the anisotropy parameter provided the group-centric distances are scaled by r_s , the characteristic radius of the NFW-profile of the host. Fossil groups are assumed to be early formed systems (see e.g. D’Onghia et al. 2005) with high concentrations. Our fitting formula implies that at a fixed radius more concentrated hosts generate more radially anisotropic velocity dispersions. This result has to be taken into account if the velocity dispersions of different groups are compared at physically similar radii.

ACKNOWLEDGEMENTS

The authors would like to thank the anonymous referee for the constructive comments which helped to improve the text. Useful discussions with Juerg Diemand and Stelios Kazantzidis are highly appreciated. This work has been supported by NSF grant AST 00-98351 and NASA grant NAG5-13275 for which we are very grateful.

REFERENCES

Benatov L., Rines K., Natarajan P., Kravtsov A., Nagai D., 2006, MNRAS, 370, 427
 Bertschinger E., 1985, ApJS, 58, 39

Binney J., Tremaine S., 1987, Galactic dynamics. Princeton, NJ, Princeton University Press, 1987, 747 p.
 Boylan-Kolchin M., Ma C.-P., 2007, MNRAS, 374, 1227
 Bryan G. L., Norman M. L., 1998, ApJ, 495, 80
 Bullock J. S., Kolatt T. S., Sigad Y., Somerville R. S., Kravtsov A. V., Klypin A. A., Primack J. R., Dekel A., 2001, MNRAS, 321, 559
 Bullock J. S., Kravtsov A. V., Weinberg D. H., 2000, ApJ, 539, 517
 Bullock J. S., Kravtsov A. V., Weinberg D. H., 2001, ApJ, 548, 33
 Chandrasekhar S., 1943, ApJ, 97, 255
 Colpi M., Mayer L., Governato F., 1999, ApJ, 525, 720
 Da Rocha C., Mendes de Oliveira C. L., 2005, MNRAS, 364, 1069
 Dehnen W., McLaughlin D. E., 2005, MNRAS, 363, 1057
 Diemand J., Moore B., Stadel J., 2004, MNRAS, 352, 535
 Diemand J., Moore B., Stadel J., 2004a, MNRAS, 353, 624
 D’Onghia E., Sommer-Larsen J., Romeo A. D., Burkert A., Pedersen K., Portinari L., Rasmussen J., 2005, ApJ, 630, L109
 Eke V. R., Navarro J. F., Frenk C. S., 1998, ApJ, 503, 569
 Hansen S. H., Moore B., 2006, New Astronomy, 11, 333
 Faltenbacher A., Diemand J., 2006, MNRAS, 369, 1698
 Faltenbacher A., Kravtsov A. V., Nagai D., Gottlöber S., 2005, MNRAS, 358, 139
 Faltenbacher A., Mathews W. G., 2005, MNRAS, 362, 498
 Hayashi E., Navarro J. F., Power C., Jenkins A., Frenk C. S., White S. D. M., Springel V., Stadel J., Quinn T. R., 2004, MNRAS, 355, 794
 Hoeft M., Mücke J. P., Gottlöber S., 2004, ApJ, 602, 162
 Islam R. R., Taylor J. E., Silk J., 2003, MNRAS, 340, 647
 Jones L. R., Ponman T. J., Horton A., Babul A., Ebeling H., Burke D. J., 2003, MNRAS, 343, 627
 Kazantzidis S., Mayer L., Mastropietro C., Diemand J., Stadel J., Moore B., 2004, ApJ, 608, 663
 Khosroshahi H. G., Maughan B. J., Ponman T. J., Jones L. R., 2006, MNRAS, 369, 1211
 Koushiappas S. M., Zentner A. R., Walker T. P., 2004, Phys. Rev. D, 69, 043501
 Kravtsov A. V., Gnedin O. Y., Klypin A. A., 2004, ApJ, 609, 482
 Lacey C., Cole S., 1993, MNRAS, 262, 627
 Macciò A. V., Moore B., Stadel J., Diemand J., 2006, MNRAS, 366, 1529
 Mahdavi A., Trentham N., Tully R. B., 2005, AJ, 130, 1502
 Mathews W. G., Chomiuk L., Brighenti F., Buote D. A., 2004, ApJ, 616, 745
 Mendes de Oliveira C. L., Cypriano E. S., Sodr e L. J., 2006, AJ, 131, 158
 Mulchaey J. S., 2000, ARA&A, 38, 289
 Navarro J. F., Frenk C. S., White S. D. M., 1997, ApJ, 490, 493
 Osmond J. P. F., Ponman T. J., 2004, MNRAS, 350, 1511
 Ponman T. J., Allan D. J., Jones L. R., Merrifield M., McHardy I. M., Lehto H. J., Luppino G. A., 1994, Nature, 369, 462
 Reed D., Gardner J., Quinn T., Stadel J., Fardal M., Lake G., Governato F., 2003, MNRAS, 346, 565
 Reed D., Governato F., Quinn T., Gardner J., Stadel J., Lake G., 2005, MNRAS, 359, 1537
 Somerville R. S., Primack J. R., 1999, MNRAS, 310, 1087

- Sommer-Larsen J., 2006, MNRAS, 369, 958
 Spergel D. N., Bean R., Dore' O., Nolte M. R., Bennett C. L., et al. 2006, ArXiv Astrophysics e-prints [astro-ph/0603449](#)
 Tasitsiomi A., Kravtsov A. V., Gottlöber S., Klypin A. A., 2004, ApJ, 607, 125
 Taylor J. E., Babul A., 2001, ApJ, 559, 716
 Taylor J. E., Babul A., 2004, MNRAS, 348, 811
 Tormen G., 1997, MNRAS, 290, 411
 van den Bosch F. C., Yang X., Mo H. J., Norberg P., 2005, MNRAS, 356, 1233
 Wechsler R. H., Bullock J. S., Primack J. R., Kravtsov A. V., Dekel A., 2002, ApJ, 568, 52
 Wojtak R., Lokas E. L., Gottlöber S., Mamon G. A., 2005, MNRAS, 361, L1
 Zabludoff A. I., Mulchaey J. S., 1998, ApJ, 496, 39
 Zabludoff A. I., Mulchaey J. S., 2000, ApJ, 539, 136
 Zentner A. R., Berlind A. A., Bullock J. S., Kravtsov A. V., Wechsler R. H., 2005, ApJ, 624, 505
 Zentner A. R., Bullock J. S., 2003, ApJ, 598, 49
 Zhang B., Wyse R. F. G., Stiavelli M., Silk J., 2002, MNRAS, 332, 647
 Zhao D. H., Mo H. J., Jing Y. P., Börner G., 2003, MNRAS, 339, 12

written as

$$\hat{u}(x) = u(xr_s) = \exp \{2b {}_2F_1[a, a, 1 + a, -x]\} \quad (16)$$

where ${}_2F_1$ is the hyper-geometric function and $x = r/r_s$ as introduced in the foregoing equation. Finally, the mass weighted mean velocity dispersion within the radius r is given as

$$\bar{\sigma}(r) = \frac{\int_0^r \rho(r') \sigma_r^2(r') r'^2 dr'}{\int_0^r \rho(r') r'^2 dr'} \quad (17)$$

The mean velocity dispersions represented by the thin lines in Fig. 5 are computed on the assumption that the matter distribution follows a NFW-density profile with a virial mass of $3.9 \times 10^{13} M_\odot$. As seen in Fig. 1 up to 10 per cent of all the particles are located outside the virial radius at $z = 0$. This particle deficit at large radii may explain the ~ 5 per cent deviations between the velocity dispersions obtained from the model and the Jeans equation ($r \leq 1.00R_{vir}$ line in Fig. 5).

APPENDIX: INTEGRATION OF THE JEANS EQUATION

Fig. 5 compares the velocity dispersions from our dynamical model with the predictions of the Jeans equation. For a spherical symmetric and static ($\bar{\sigma}_r = \bar{\sigma}_t = 0$, no mean radial or tangential motions) system the Jeans equation can be written as

$$\frac{1}{\rho} \frac{d}{dr} (\rho \sigma_r^2) + 2\beta \frac{\sigma_r^2}{r} = -\frac{d\Phi}{dr} \quad (12)$$

where ρ is the density, σ_r is the radial velocity dispersion, Φ is the gravitational potential and β is the anisotropy parameter (see e.g. Binney & Tremaine 1987). A solution of this first order differential equation can be obtained by means of multiplying both sides of the Eq. 12 by the integrating factor

$$u(r) = \exp \left[2 \int_0^r \frac{\beta(r') dr'}{r'} \right] \quad (13)$$

and performing an integration from a given radius r to infinity. The application of the boundary condition $\lim_{r \rightarrow \infty} \sigma_r^2 = 0$ which any ordinary bound system satisfies results in

$$\begin{aligned} \rho(r) \sigma_r^2(r) \exp \left[2 \int_0^r \frac{\beta(r') dr'}{r'} \right] \\ = \int_r^\infty \frac{d\Phi}{dr}(r') \rho(r') \exp \left[2 \int_0^{r'} \frac{\beta(r'') dr''}{r''} \right] dr' \quad (14) \end{aligned}$$

For completeness we repeat the fitting formula for the anisotropy parameter β as given in Eq. 11

$$\beta(r) = b \left(\frac{x}{x+1} \right)^a \quad x = r/r_s, \quad (15)$$

where r_s is the scale factor of the NFW-profile. With this expression for $\beta(r)$ the integrating factor (Eq. 13) can be